V_S^{30} mapping and soil classification for seismic site effect evaluation in Dinar region, SW Turkey

Ali Ismet Kanlı,[1] Péter Tildy,[2] Zsolt Prónay,[2] Ali Pınar[1] and László Hermann[2]

[1]*Istanbul University, Engineering Faculty, Department of Geophysical Engineering*, 34320, *Avcılar, Istanbul, Turkey. E-mail: kanli@istanbul.edu.tr*
[2]*Eotvos Lorand Geophysical Institute, Department of Engineering Geophysics, Budapest, Hungary*

SUMMARY

The Dinar earthquake ($M_S = 6.1$) of 1995 October 1 killed 90 people and destroyed more than 4000 buildings. Despite the moderate size of the earthquake, the level of damage was extremely high, which led to many studies that were carried out in the region. The majority of these studies concluded that the main reasons for the damage were the construction errors and the poor soil conditions. However, at that time no appropriate soil condition map based on extended, high density measurements was available.

Shear wave velocity is an important parameter for evaluating the dynamic behaviour of soil in the shallow subsurface. Thus site characterization in calculating seismic hazards is usually based on the near surface shear wave velocity values. The average shear wave velocity for the top 30 m of soil is referred to as V_S^{30}. For earthquake engineering design purposes, both the Uniform Building Code (UBC) and Eurocode 8 (EC8) codes use V_S^{30} to classify sites according to the soil type.

The V_s^{30} values calculated by using multichannel analysis of surface waves (MASW) were used to create a new soil classification map of the Dinar region. Surface seismic measurements were carried out at 50 locations mostly in Dinar city and its surroundings. The dispersion data of the recorded Rayleigh waves were inverted using a Genetic Algorithm (GA) method to obtain shear wave velocity profiles of the investigated sites. Thus the derived V_s^{30} map of the Dinar region was transformed to the UBC and EC8 standards.

Soil classification results show that most parts of the region, located in alluvial basin, have low shear wave velocity values. These values are within the range of 160–240 m s^{-1} and thus fall into the S_D and S_E categories according to the UBC and the C and D categories according to EC8. Within the region, some parts located on the hill zone and the transition zone have better soil conditions [corresponding to S_C (UBC) and B (EC8) categories] and have comparatively high shear wave velocities in the range of 500–740 m s^{-1} and 350–450 m s^{-1}, respectively. V_S^{30} and soil classification maps were compared with the damage distribution associated with the earthquake. In possession of a detailed shear wave velocity map of Dinar City, in general, the results show that there is a correlation between the V_S^{30} values and the damage distribution of the region. In addition to the low V_S^{30} values, the likely causes of the damage were investigated, and it is observed that one of the major factors for high levels of damage is 3-D variations of geological structures.

Key words: Eurocode 8, genetic algorithms, multichannel analysis of surface waves, soil classification, Uniform Building Code, V_S^{30}.

1 INTRODUCTION

Dinar has a history going back to about 1200 BC. In the 8th century King Midas made Dinar the capital of his kingdom (Çatal 1997). The city is located in the 'Region of Lakes' of South-West Anatolia Region on 38.06° longitude and 30.15° latitude (Fig. 1). The

region is in highly seismically active Aegean extensional domain (Taymaz *et al.* 1991; Wright *et al.* 1999). The Dinar earthquake (1995 October 1, $M_S = 6.1$) took place in a horst–graben system. Due to the complex movements of major blocks in the vicinity of Dinar, the area is opening up in the NE–SW direction because of compression in the NW–SE direction. The area under consideration
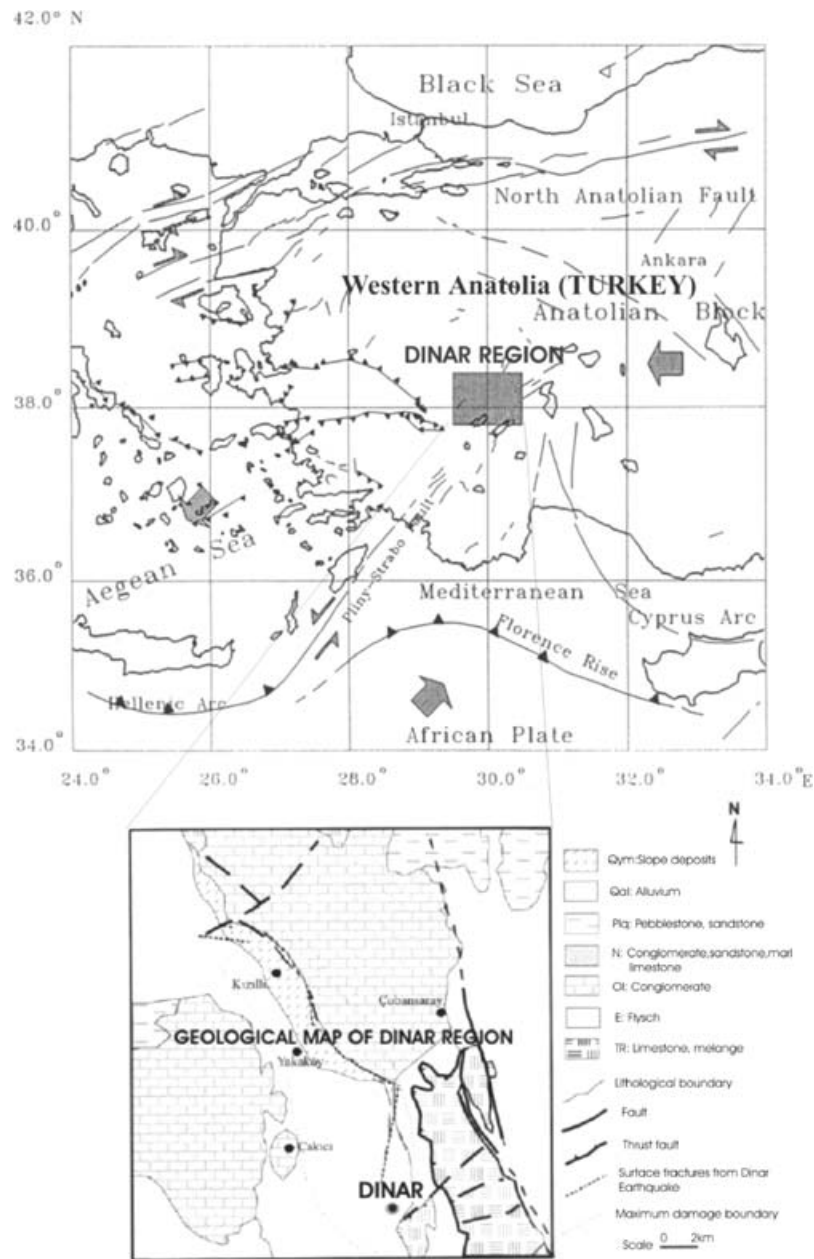
GJI Seismology

Figure 1. General tectonic features of Western Anatolia and geological map of Dinar Region (compiled from Barka 1992; Pınar 1998; Öncel *et al.* 1998).

is dissected by a multitude of NE–SW trending faults of normal and possibly strike-slip motion (Eyidogan & Barka 1996; Durukal *et al.* 1998; Pınar 1998).

The moderate-sized earthquake killed 90 people and destroyed more than 4000 buildings. The instrumentally-located epicentre of the Dinar earthquake was 38.13°N–30.08°E, about 3 km north of the city of Dinar. The focal depth was at 24 km and the duration of strong motion was 25 s. The intensity of the shaking in Dinar was VIII according to the Modified Mercalli Intensity (MMI) scale (Demirtaş *et al.* 1995; Kayabalı 1997). The hanging wall near the city was downthrown (SW) about 25–30 cm after the earthquake. Although the general trend of the surface ruptures was 130°–140°, with predominantly normal faulting character, minor strike-slip components were also observed (Eyidogan & Barka 1996).

Despite the moderate size of the Dinar earthquake, the consequent high levels of damage in the region motivated many people to carry out studies related to the geotechnical site conditions, soil liquefaction, damage distribution, earthquake characteristics and the soil properties in Dinar and its surroundings.

According to these studies (e.g. Bakır *et al.* 2002; Durukal *et al.* 1998; Öncel *et al.* 1998) there are three main zones in Dinar, based on level of damage and geology.

(1) Zone 1. The eastern part of the city, characterized by low level of damage. The hills at the east of Dinar define this zone. Mainly composed of Eocene and Oligocene aged limestone and conglomerates.

(2) Zone 2. This area of the city suffered the highest damage. It can be divided into two parts (Sucuoğlu *et al.* 2003): The first part is the transition zone from the hills to the alluvial plain, composed of stiff soil overlying the dipping limestone interface; the second is located on deeper quaternary alluvium deposits carried by the Büyük-Menderes river, containing sand, gravel and clay over the limestone bedrock. Resistivity surveys conducted in the Dinar plain by Özpınar (1978) indicated that the thickness of unconsolidated materials underlying the plain ranges from a few tens of meters to depths of 250 m.

(3) Zone 3. The western part of the city characterized by lower level of damage than Zone 2. This zone is also flat, its geotechnical properties are similar to Zone 2, but the buildings are of different type.

The ground water table is located within a few meters of the surface of the plain. Below the surface there are many underground creeks and rivers running northward, especially in the western part of Dinar (Tezcan & Ipek 1996).

The severe damage caused by the earthquake was explained as follows:

(1) Reinforced concrete buildings are located on soft soil of the lower basin of Dinar (elevations lower than 870 m). The influence of soil conditions on the degree of damage was very clear. Almost half of the city located on the sloping hills of eastern Dinar where the ground consists of hard limestone (elevations from 880–940 m) suffered practically no damage (Tezcan & Ipek 1996).

(2) The damage distribution observed in the region clearly demonstrates the effect of local site conditions and soil amplification arising from the geological and geotechnical factors (Ansal *et al.* 2001).

(3) In the computations of intensity distribution, the geotechnical site conditions play an important role where rock sites produce consistently lower ground-motion intensities than the less stiff sites (Sucuoğlu *et al.* 2003).

(4) The main causes underlying the severity of the structural damage were the construction errors and the poor dynamic characteristic of alluvial soils. The importance of soil conditions is represented by the moderate damage on strong soil areas in the northern part of Dinar (Çatal 1997).

(5) As observed from the borehole logs, the composition and characteristics of alluvium are highly variable over short vertical and lateral distances. Investigations of site response through 1-D and 2-D methods led to the conclusion that the 1-D response analysis underpredicts the amplification in the heavy damaged zones. The differences between the peaks of respective spectral accelerations calculated by the 1-D and 2-D methods increase with increasing shear wave velocities of the soil profile, and they decrease with increasing distance from the rock outcrop. These results suggest the important role of basin edge effect in the observed damage distribution (Bakir *et al.* 2002).

It can be seen that the majority of studies concluded that one of the main reasons for such severe damage was the soil conditions. Although several boreholes were drilled, and standard penetration tests (SPT) (Clayton 1995) performed in different sections of the city, there were insufficient investigations (mainly in the city centre) to enable an extended soil condition map to be drawn. There is obviously a need for an extensive, homogeneous data set to describe the soil conditions of the region.

2 METHODOLOGY

Elastic properties of near-surface materials and their effects on seismic wave propagation are very important in earthquake and civil engineering, and in environmental and earth science studies. The increase of amplitudes in soft sediments is one of the most important factors responsible for the amplification of earthquake motions. Amplification is proportional to

$$\frac{1}{\sqrt{V_s \cdot \rho}}, \tag{1}$$

where V_s is the shear wave velocity and ρ is the density of the investigated soil (Aki & Richards 1980). Since density is relatively constant with depth, the V_s value can be used to represent site conditions. A thorough assessment of shallow shear wave velocity is crucial for earthquake-hazard assessment studies (Wald & Mori 2000).

The average shear wave velocity of the upper 30 m ($V_s{}^{30}$) should be computed in accordance with the following expression:

$$V_s{}^{30} = \frac{30}{\sum_{i=1}^{N}(h_i/v_i)}, \tag{2}$$

where h_i and v_i denote the thickness (in meters) and shear-wave velocity (at a shear strain level of 10^{-5} or less) of the *i*th formation or layer, in a total of N, existing in the top 30 m. $V_s{}^{30}$ was accepted for site classification in the USA (NEHRP) by the UBC (Uniform Building Code) in 1997 (Dobry *et al.* 2000), and also in the new provisions of Eurocode 8 (Sabetta & Bommer 2002; Sêco e Pinto 2002).

The UBC classification was applied for site condition mapping in California (Wills *et al.* 2000). The determinations of V_s data were carried out in boreholes, using downhole or crosshole methods. Such measurements are not cost-effective because several boreholes need to be drilled, and this tends to cause difficulties in urban areas. Surface seismic methods, the best alternatives to borehole measurements, are also applicable for velocity determination. P and S reflection/refraction data were used for compressional and shear wave velocity determination in Seattle (Williams *et al.* 1999). However, refraction methods cannot handle velocity inversions and close refractors (hidden layers). The data may be very sensitive to heavy traffic and artificial environment (basements of buildings, cellars, drains and sewers). In addition, long arrays are necessary for deep investigations, which make it difficult to find suitable locations for measurements in urban areas.

In recent years, the possibilities of surface wave analysis have been increased with the development of powerful computers. This type of analysis is based on the dispersive nature of surface waves in layered or heterogeneous media.

3 SURFACE WAVE ANALYSIS

Although ground roll is considered as noise in conventional body wave surveys, its dispersive properties can be used to obtain information related to near-surface elastic properties (Nazarian *et al.* 1983; Stokoe *et al.* 1994; Park *et al.* 1998). Of all types of seismic waves, surface waves have the strongest energy by virtue of which they have the highest signal-to-noise ratio (S/N) (Park *et al.* 2002), making it a powerful tool for near surface characterization.

In layered media, the propagation velocity of a surface wave depends on the frequency (or wavelength) of the wave because of
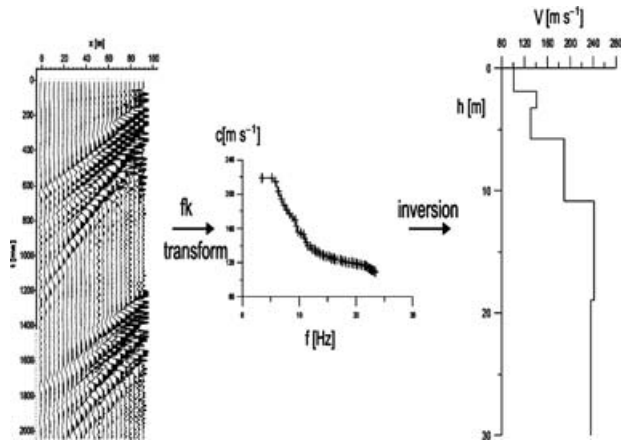
Figure 2. Main steps of the MASW processing technique. (Data acquired from profile 27).

Figure 3. Multichannel record showing different wavetypes.

geometric dispersion. Shear wave velocity can be derived from inverting the phase velocity of the surface (Rayleigh and/or Love) waves (Dorman & Ewing 1962; Aki & Richards 1980) (Fig. 2).

Several types of surface wave methods have been proposed for near-surface characterization by using a great variety of testing configurations, processing techniques, and inversion algorithms. In general, two widely-used techniques are preferred: SASW (Spectral Analysis of Surface Waves) and MASW (Multichannel Analysis of Surface Waves).

In the early stages of surface wave analysis, only one pair of receivers was used with different spacings. The traveltime between the receivers was calculated from phase differences (Nazarian & Stokoe 1984). This method was widely used in geotechnical projects (e.g. Stokoe *et al.* 1994) but it is very sensitive to noise and the coupling of the receivers. During the dispersion curve estimation the unwrapping of the cross power spectrum phase is a critical step. The interference of different wave types may easily lead to the misinterpretation of phase velocities. In addition, repeated measurements are needed in the field.

In contrast, most of these disadvantages are overcome by MASW (Park *et al.* 1999). The field work is much easier and the measurement time is strongly reduced. Multichannel records make it possible to separate different wavefields in the f–k domain. In some cases, it is possible to analyse fundamental and higher modes simultaneously, thereby consistently providing more accurate shear wave velocities. Often only the fundamental mode is used because it has the highest energy among all wave types.

All variations of multichannel surface wave methods are environment-friendly, non-invasive, low-cost, rapid and robust, and—moreover—they consistently provide reliable Shear wave velocity profiles within the first 30 m below the surface (Xia *et al.* 2002).

The large amount of geotechnical data accumulated in previous studies give us an opportunity for proving the effectiveness of the method in $V_s{}^{30}$ mapping, comparing the results with these data, and with the damage distribution of the Dinar region (Kanlı *et al.* 2004).

4 FIELD STUDY AND DATA ACQUISITION

Although the acquisition of ground roll data seems to be an easy task, field configurations need to be optimized for the requirements.
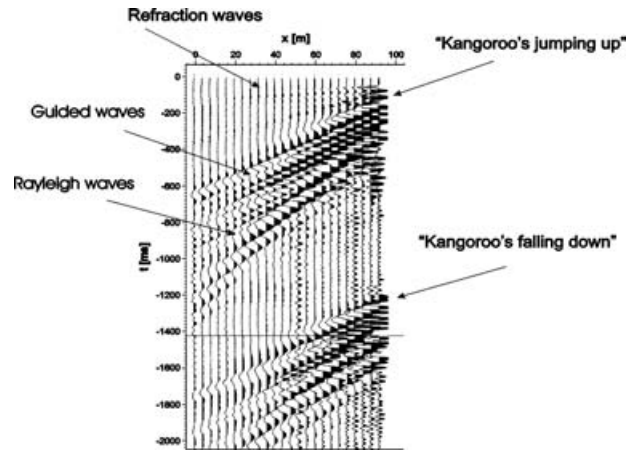
Our main objective was to cover the whole area of the city and its surroundings. Taking into account the number of records needed, and the time-frame available for the field work, the method and measurement system had to be reliable and robust. Our task was to image the shear wave velocity of subsurface layers down to at least 30 m, so the frequency content of the records had to be low enough to obtain phase velocities at large wavelengths as well. Usually the fundamental mode Rayleigh wave dominates the f–k spectrum, thus the seismic array (including the type of source and receivers, offset and spacing) was optimized to obtain the fundamental mode in accordance with our earlier experience and the literature (Tildy *et al.* 2003; Park *et al.* 2002). The seismic source and the subsurface structure generate a huge variety of other wave types such as direct, refracted and reflected *P* and *S* waves, as well as guided, converted and higher mode Rayleigh waves (Fig. 3). The field record contains both ambient and traffic noise mainly in urban areas. The most important parts of the field configurations are the geophone spacing and the offset range. The planar characteristics of surface waves evolve only after a certain distance from the source. In most cases, this distance needs to be greater than the half of the maximum desired wavelength (Stokoe *et al.* 1994). On the other hand, the amplitude of body and higher mode Rayleigh waves may dominate over the fundamental mode at high frequencies. The relationship between the energy of fundamental and higher modes is a complex function of layer parameters and offset but, as a rule of thumb, the maximum distance between the source and the furthest geophone should not exceed 100 m (Park *et al.* 2002).

The acquisition layout is an array of vertical geophones with equal spacing. The natural frequency of geophones is very important for data quality. The lower frequency of signals means that a longer wavelength of surface waves is recorded which, in turn, results in a larger depth of investigation.

A special source called SR-II (Kangaroo) was used for our field measurements (Fig. 4), developed by ELGI (Eötvös Loránd Geophysical Institute of Hungary). The weight of this source is 80 kg and it is operated by a blank 12-bore shotgun cartridge that is fired by an electric starter device. The weight of the source acting as a reaction mass creates a more efficient coupling to the ground. Despite its heavy weight, it can jump up to a height of 2 m. The source was developed for reflection seismic measurements but it generates strong Rayleigh waves as well. The amplitude spectrum of a shot gathered by a broad-band seismograph (CMG-40T type) can be seen in Fig. 5. Since the spectrum of the amplitude is rather flat in the

Figure 4. SR-II (Kangaroo) in action.

0.3–30 Hz frequency range, it makes the Kangaroo a good source for 'surface waves' studies. The sharp decrease of amplitudes in the figure near 30 Hz is the cut-off frequency used in the spectral analysis.

In addition to the surface wave data acquisition, P wave refraction measurements were also carried out. The results of seismic refraction measurements provide constraints for model parameters improving thereby the reliability of the surface wave inversion process. The main parameters for data acquisition are given in Table 1.

5 DATA PROCESSING

Data processing consists of two main steps: (i) Obtaining the dispersion curves of Rayleigh wave phase velocity from the records;
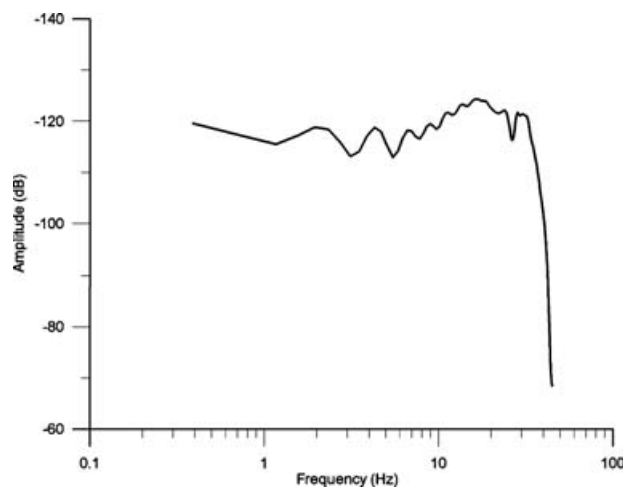

Figure 5. Amplitude spectrum of a Kangaroo shot recorded by (CMG-40T type) broadband seismograph.

Table 1. Data acquisition parameters.

	Seismic refraction	Surface waves
Number of channels	24	24
Geophone spacing	4 m	4 m
Array length	92	92
Sampling rate	0.5 ms	0.5 ms
Record length	1024 ms	2048 ms
Receiver	2.5 Hz vertical (spikes or plates)	2.5 Hz vertical (spikes or plates)
Source	5 kg hammer (on metal plate)	SR-II (Kangaroo)
Minimal offset	2 m	30 m

(ii) Determining the V_s profiles from which the V_s^{30} values are calculated (see Fig. 2).

Several approaches have been developed for these steps. F–k analysis and slant stack transform (McMechan & Yedlin 1981) are also used to obtain dispersion curves from multichannel records. There are different procedures available for solving the forward problem, too. The Thomson–Haskell method of the transfer matrix and the dynamic stiffness matrix (proposed by Kausel and Roesset) are the most frequent solution techniques in practice (Thomson 1950; Haskell 1953; Kausel & Roesset 1981). Also, various inversion strategies are utilized, from trial and error to global search methods. Recently, inversion of full waveform was proposed by Forbriger (Forbriger 2003a,b). This method exploits the full wavefield content, and there is no need to identify different modes prior to inversion.

5.1 Signal analysis

We carried out data processing in accordance with the characteristics of field records. Firstly, the records are muted to reduce the effect of random noise and the interference with other wave types. After muting, only the surface wave component (jumping up) of the Kangaroo is used for f–k transformation. Zero padding in the space and time domains is also applied to improve the frequency and wavenumber resolution of the f–k transformation (Foti *et al.* 2003). The dispersion curve is obtained from the (absolute and relative) maxima of the f–k spectrum. After careful analysis of the records only the fundamental mode of Rayleigh waves (from 3–5 to 30–40 Hz) was investigated. Fig. 6 shows one of the f–k spectra. The longest wavelengths obtained from the f–k spectra are in the interval from 60 to 120 m, depending on the soil structure.

The inversion method also has two steps. First, a starting model is built by interactive inversion taking into consideration only the V_s and the thickness parameters of the layered media. Then, an inversion technique based on a Genetic Algorithm (GA) (for details, see later) is applied to calculate layer parameters. The core computation of both interactive and GA inversions is the dispersion calculation based on the well-known algorithms of Thomson (1950) and Haskell (1953). The earth's structure in this method is represented by horizontal layers with their thickness (d), body wave velocities (V_S, V_P), and density (ρ).

By using this approach the phase velocity curves can be determined by the (c, f) root pairs of the following equation:

$$F(c, f) = 0, \tag{3}$$

where $F(c, f)$ is a relatively complicated function constructed from the 4×4 layer matrices. The series of (c) roots give the phase velocities of the fundamental and the higher modes at fixed frequency.
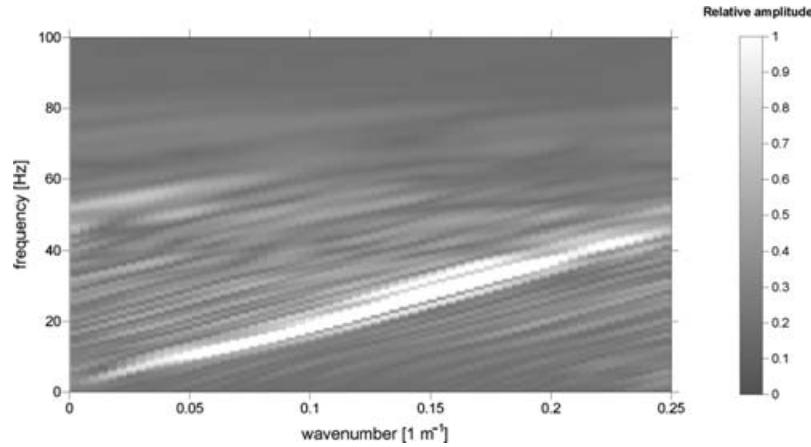
Figure 6. *F–k* spectrum at profile number 44.

All (c) values can be determined by repeating the process at all frequencies of the measured data. (Ben-Menahem & Singh 1981; Thomson 1950; Haskell 1953).

5.2 The initial model

Although GA is a global optimization method the reliability and speed of the inversion can be improved in a significant way by ensuring that the most appropriate starting model is used. Layer parameters should be close to the real ones for a good starting model. The dispersion curve $c(\lambda)$ of Rayleigh waves is a scaled and smoothed form of the shear wave velocity profile (Matthews *et al.* 1996), thus it can be approximated as,

$$V_s(z) = 1.1 \cdot c(\lambda = r \cdot z), \tag{4}$$

where z is depth, $V_s(z)$ is the shear wave velocity at depth z, $c(\lambda)$ is the phase velocity related to wavelength λ, which is equal to the multiplication of depth and, r is the depth conversion factor (between 2 and 4).

The number of layers can be estimated from the ratios λ_{max} and λ_{min} of the measured dispersion data by keeping the ratio of thickness-to-depth of a layer constant. In our experiments, 4–12 layers are used with the ratios between 0.2 and 0.4. By using this interval, the velocity V_s in each layer can be determined as a geometric mean of the measured phase velocities for $c(\lambda)$ data,

$$V_s(i) = 1.1 \cdot \sqrt{\prod_j c(\lambda(j))}, \tag{5}$$

where $V_S(i)$ is the velocity of the *i*th layer, Π is the symbol of multiplication, $c(\lambda(j))$ is the phase velocity related to the *j*th wavelength:

$$r \cdot H(i-1) < \lambda(j) < r \cdot H(i), \tag{6}$$

where $H(i)$ is the depth of the *i*th layer, and r is the depth conversion factor. The *P*-wave velocities of layers are calculated from refraction data, and the ratio ρ_i/ρ_1 is estimated from $Vp(i)/Vp(1)$.

The value of r at each measured dispersion curve can be determined by scaling down the depth data, and searching for the best (r) based on the overall goodness-of-fit between the measured and calculated dispersion curves. Having determined the scaling factor, we apply an iterative feedback to resolve the smoothness of V_s data derived from the (c) values. The iterative feedback compares measured dispersion curves with the calculated ones at the points

belonging to the layers and modifies the $V_s(i)$ value for better fitting,

$$V_s(i)' = \sqrt{\prod_j c_m(\lambda(j))/c_c(\lambda(j))} \cdot V_s(i), \tag{7}$$

where c_m and c_c mean the measured and calculated phase velocities, respectively. The number of steps of this iteration is usually 16–32.

5.3 Genetic algorithms

Genetic Algorithms (GA) are global optimization methods (Sen & Stoffa 1995) that employ a blind search technique based on the natural process of evolution. Nature defines and constructs lifeforms with genes. Geophysical parameters, e.g. thickness, *P–S* wave velocity and density, can be treated as genes. In this respect, the use of GA can be mentioned for inverting surface waves in pavement investigations (Al-Hunaidi 1998). The evolution of the parameters is controlled by the following processes:

(1) *Reproduction and crossing over*. New individuals are created and the genomes of the mating partners are mixed.

(2) *Mutation*. During the reproduction process, mutations are possible. This random event modifies chromosomes. The GA is able to create distinct new individuals using mutation, which increases the variability of chromosomes.

(3) *Selection*. 'Survival of the Fittest' means the best fit between the measured and calculated dispersion curves. Natural selection prefers, consequently, the best of a generation and as these 'bests' are able to reproduce themselves more often, they can take better care of their progeny. The next generation is thus more optimized than its predecessor.

In the inversion algorithm, an initial population is selected at random and the GA seeks to improve the fitness of the models generation after generation by the processes of reproduction, crossover, selection and mutation. In our processing sequence, the starting model is included in the initial population.

In several cases only the V_s parameters are implied in the inversion process (Xia *et al.* 1999), making it more stable. In this case, however, the velocity profiles could be used as constraints for inversion models thereby avoiding the problems of non-real structures.

To demonstrate the importance of including *P*-wave velocity to the inversion, some calculations were made by using a simple two-layered model (Fig. 7). In the calculations, V_{S1}, V_{S2}, V_{P2}, H and
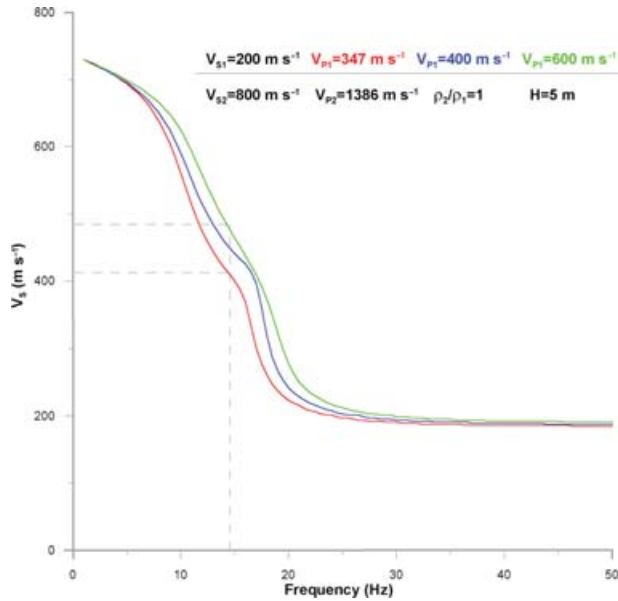
Figure 7. Dispersion curves for a simple two-layered model.

Figure 8. Decrease of error in the percentage of the starting model versus generations (iteration steps) in the Genetic Algorithm at Profile 14.

ρ_2/ρ_1 were taken as constant, the only difference was the *P*-wave velocity of the first layer. The Thomson (1950) and Haskell (1953) algorithms use both V_S and V_P for dispersion calculations. Without inverting V_P as well, some relationships are considered between V_S and V_P, in most cases the square root of 3, which can be valid for solid rock. In our case, the ratios of $\sqrt{3}$, 2 and 3 were used, respectively, between the *P*-wave and *S*-wave velocities (Fig. 7). At 14.5 Hz, the velocity difference can be as high as 80 m s^{-1}, depending on the ratio of the velocities. Because of this possible difference between the dispersion curves, which yield quite different inversion results, both *P*-wave and *S*-wave velocities are needed for the inversion.

The two synthetic seismograms with the same V_S but different V_P structure were inverted by the assumption of $V_P = \sqrt{3}V_S$. In the first case, the assumption was true and the inversion yielded the original model ($V_{S1} = 199$ m s^{-1}, $V_{S2} = 802$ m s^{-1}, $H = 5.04$ m). In the second case, the *P*-wave velocity in the first layer was $V_{P1} = 3V_{S1}$, while the other parameters were unchanged. The results were obtained as, $V_{S1} = 223$ m s^{-1}, $V_{S2} = 803$ m s^{-1}, $H = 4.44$ m, respectively. The depth error is more than 10 per cent caused by the incorrect *P* velocity in the first layer.

Constraints on layer parameters are generally applied and the joint inversion of various data are undertaken, e.g. Rayleigh dispersion and *P* wave. Other restrictions are the application of lower and upper limits on all parameters, and that the ratio of V_P/V_S must be greater than $\sqrt{3}$ for physical reasons.

In this study, the population consists of 50 members and the number of generations is 50; and our objective is to obtain the best fitted layer model. The misfit (error) is defined as the sum of the squares of the difference of the measured and calculated values divided by the frequency. The reason for this process is that the dispersion data are equally sampled in the frequency domain. This means that in the depth domain, shallow depths (high frequencies) are over-represented. To avoid the process being dominated by the shallow artefacts, their weight is reduced in the misfit calculations by weighting with 1/f. The typical decrease of errors can be seen in Fig. 8 at Profile 14.
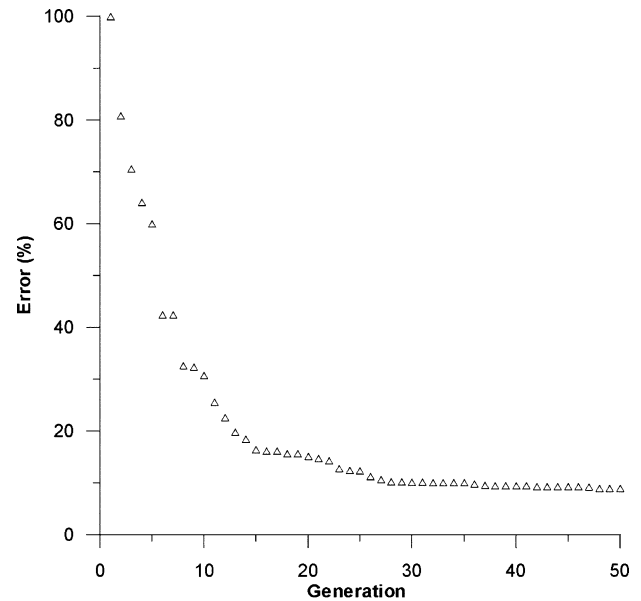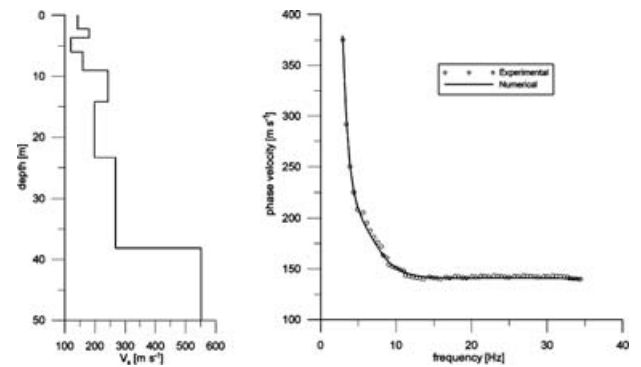

Figure 9. Velocity profile and comparison of experimental and numerical dispersion curves at Profile 44.

In the first iterations, the error decreases rapidly. In some generations, the error is constant because no better solution is created. The convergence is fast but not monotonic, there are some steps on the function. In Fig. 9 the experimental dispersion is compared with the numerical one for the last iteration of the inversion process. The resulting model can also be seen. The experimental curve is obtained from the *f*–*k* spectrum shown in Fig. 6.

6 SHEAR WAVE VELOCITY DISTRIBUTION OF THE REGION

The calculated shear wave velocity distribution down to a depth of 30 m of Dinar and its surroundings can be seen in Fig. 10. Light-blue numbers mark the locations of the 50 measuring points on the figure. The V_S^{30} distribution is overlaid by the Dinar settlement map that includes both the present state and the future plans of the Dinar Municipality.

Three different velocity zones exist. These zones coincide very well with the topography (Fig. 11), and are very similar to zones identified in previous studies. In general, high and medium shear
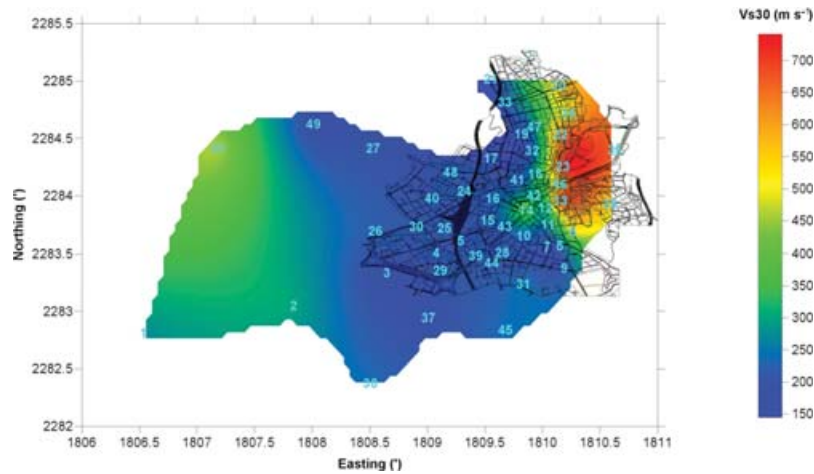
Figure 10. $V_S{}^{30}$ distribution map of Dinar and its surroundings.
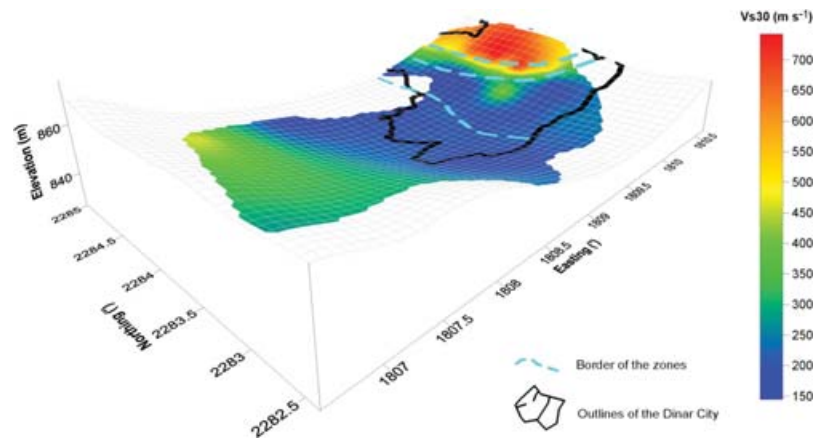

Figure 11. $V_s{}^{30}$ distribution values overlaid on the simplified 3-D topographic map of Dinar and its surroundings. (Vertical scale is exaggerated. The difference between the maximum and minimum of Z axis is only 40 m, the length of the X axis is approximately 6 km).

wave values correspond to the hill zone and transition zone while lower ones correspond to the basin. Most of the Dinar region is located on the flat alluvial basin, exposed to the heaviest damage during the 1995 October 1 Dinar earthquake. This zone is located in the flat alluvial basin in the north–south and west directions (blue-coloured zone) characterized by very low shear wave velocity values (between 150 and 250 m s^{-1}). The transition zone (green coloured) is a rather high velocity zone (between 350 and 450 m s^{-1}), which extends in the north–south direction. The hill zone (light yellow to red-coloured zone) in the eastern part of the region has the highest velocity values (between 500 and 740 m s^{-1}) throughout the region.

The $V_S{}^{30}$ distribution map, especially the lowest velocity zones, coincides with the previous results of geotechnical and geophysical investigations and borehole logs. The standard penetration test (SPT) results, which are mainly used to estimate the relative stiffness and strength (bearing capacity) of soils, are available in the alluvial basin, the blow counts are 4–20 in the first 5 m and 20–50 in the second 15 m. Accordingly, sand and gravel series can be classified as loose and medium dense in the two consecutive layers, respectively (Sucuoğlu *et al.* 2003). SPT blow counts can be as low as 2–5 in the first 10 m depth in the heavily damaged zone. In the next 20 m, the blow counts

are rarely below 15 in any of the boreholes (Bakir *et al.* 2002). For comparison, SPT blow counts were calculated from our V_S values by using the equation and data from Ansal *et al.* (2001). Both SPT and equivalent shear wave velocity values correlate with our results (Kanlı *et al.* 2004).

Three velocity-depth profiles can be seen in Fig. 12. These profiles represent the most important zones in the Dinar region Profile 35 and Profile 27 are located in the hill zone and in the alluvial basin, respectively, and Profile 14 (near the transition zone) is a special one.

Profile 35 (hill zone) shows a normal two-layer model with a small velocity inversion, possibly some fracturing, in the unweathered and undamaged rock. The solid rock is below 28 m or there is a change in the rock type. In Profile 27, located in the alluvial basin, the main reason for velocity changes is the weak compaction of the sediments down to about 12 m. The low velocity at greater depth shows that the alluvium is not densely packed. In Profile 14, there is a very low velocity layer near the surface. However, the velocity increases until the basement is reached except for an anomalous high velocity zone. This zone significantly affects the $V_S{}^{30}$ value. The location belongs to one of the high levels of the damaged areas despite $V_s{}^{30}$ being rather high.
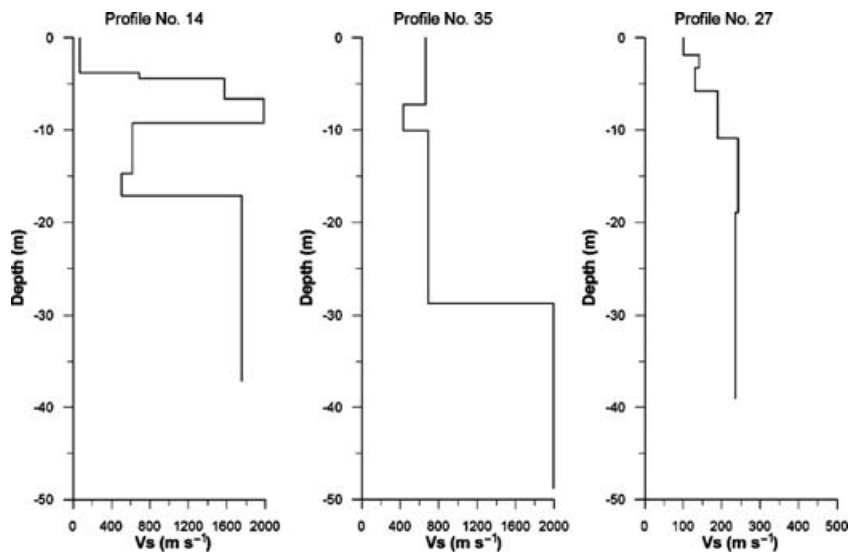
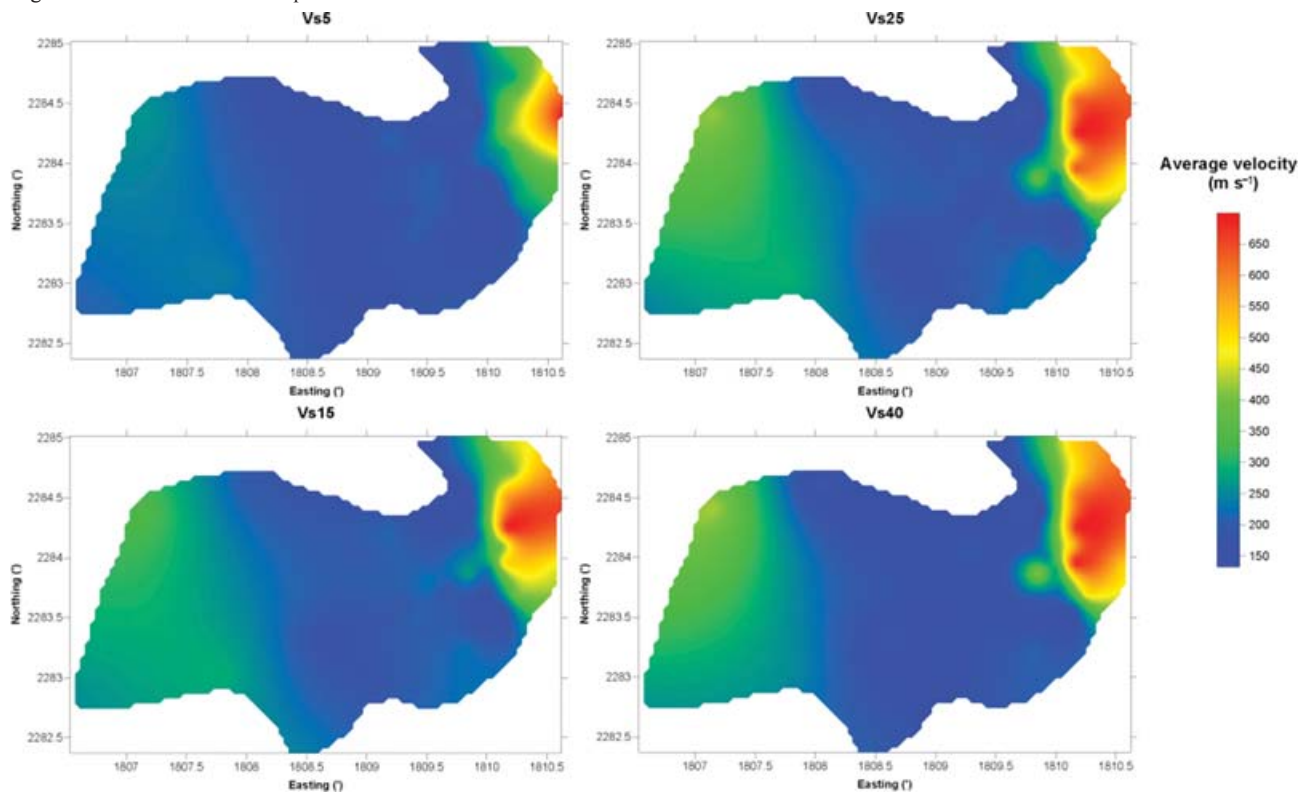**Figure 12.** Selected results of dispersion curve inversions.

Figure 13. Average shear wave velocity distribution maps of Dinar and its surroundings down to 5 (V_S^5), 15 (V_S^{15}), 25 (V_S^{25}) and 40 (V_S^{40}) meters depth, respectively.

In order to figure out the average shear wave velocity distribution with depth, different velocity distribution maps were obtained at four different depths, 5, 15, 25 and 40 m, respectively (Fig. 13). In general, there is no abrupt change in the shear wave velocity values in the alluvial basin but the changes in the values can be seen clearly on the hill and transition zone as we go down to deeper layers.

The set of average V_s values to certain depths shows that the top layer, even on the hill, is rather loose. Moving downwards the velocity increases except in the basin where there are only small variations with depth. The mentioned anomaly is clearly visible at the depth of 25 m. Its influence decreases below 40 m. The average velocities are highly affected by the near surface low velocity layers. Even on the hill, there is a thin, low velocity layer and a weathered zone of 10–30 m above the solid rock.

7 SOIL CLASSIFICATION

An important part of this study is the soil classification of Dinar city and its surroundings. Although only the settlement of Dinar

Table 2. Ground profile (soil) types or classification of subsoil classes according to UBC (Uniform Building Code) and EC8 (Eurocode 8) standards based on the V_s^{30} values (modified from Sêco e Pinto 2002; Dobry *et al.* 2000; Sabetta & Bommer 2002).

Ground profile (Soil) type (UBC) or Subsoil Class (EC8)	Ground description (UBC)	Description of stratigraphic profile (EC8)	Shear wave velocity V_s^{30} (m s^{-1})
S_A(UBC)	Hard rock	—	>1500 (UBC)
S_B(UBC) or A (EC8)	Rock	Rock or other rock-like geological formation, including at most 5m of weaker material at the surface	760–1500 (UBC) or >800 (EC8)
S_C(UBC) or B (EC8)	Very dense soil and soft rock	Deposits of very dense sand, gravel or very stiff clay, at least several tens of m in thickness, characterized by a gradual increase of mechanical properties with depth	360–760 (UBC) or 360–800 (EC8)
S_D(UBC) or C (EC8)	Stiff soil	Deep deposits of dense or medium-dense sand, gravel or stiff clay with thickness from several tens to many hundreds of m.	180–360 (UBC and EC8)
S_E(UBC) or D (EC8)	Soft soil	Deposits of loose-to-medium cohesionless soil (with or without some soft cohesive layers), or of predominantly soft-to-firm cohesive soil	<180 (UBC and EC8)
S_F(UBC) or E (EC8)	Special soils	A soil profile consisting of a surface alluvium layer with V_s^{30} values of class C or D and thickness varying between about 5 m and 20 m, underlain by stiffer material with $V_s^{30} > 800$ m s^{-1}	—
S_1 (EC8)	—	Deposits consisting—or containing a layer at least 10 m thick—of soft clays/silts with high plasticity index ($PI > 40$) and high water content	<100 (EC8)
S_2 (EC8)	—	Deposits of liquefiable soils, of sensitive clays, or any other soil profile not included in classes A–E or S_1	— (EC8)
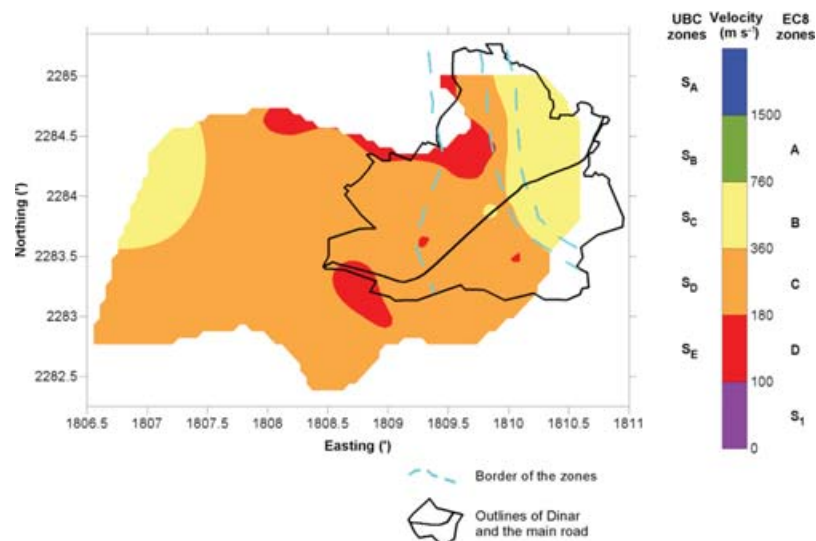
Figure 14. Soil classification map of Dinar and its surroundings according to UBC (Uniform Building Code) and EC8 (Eurocode 8) standards based on the average shear wave velocity distribution down to 30 m.

city is important in terms of seismic safety studies, a larger area is investigated and classified according to UBC and EC8 standards (see Table 2), taking into account the future settlement planning in the region. As seen in the soil classification map of Dinar and its surroundings (Fig. 14), a large part of the city belongs to the S_D category according to UBC and the C category according to the EC8 standards. There are also small parts of the region which are located on the transition zone and the hill zone that have bet-

ter soil conditions corresponding to S_C (UBC) and B (EC8) categories. These parts have higher velocity values when compared with the flat alluvial basin. Only small areas belong to S_E and D categories according to the EC8 and UBC standards. On the map (Fig. 14), both the outlines of Dinar and the high levels of damaged area (between light-blue dotted lines) can be seen. According to the map, this area includes all S_D-C (UBC-EC8), S_C-B (UBC-EC8) and S_E-D (UBC- EC8) soil type categories. Some parts of
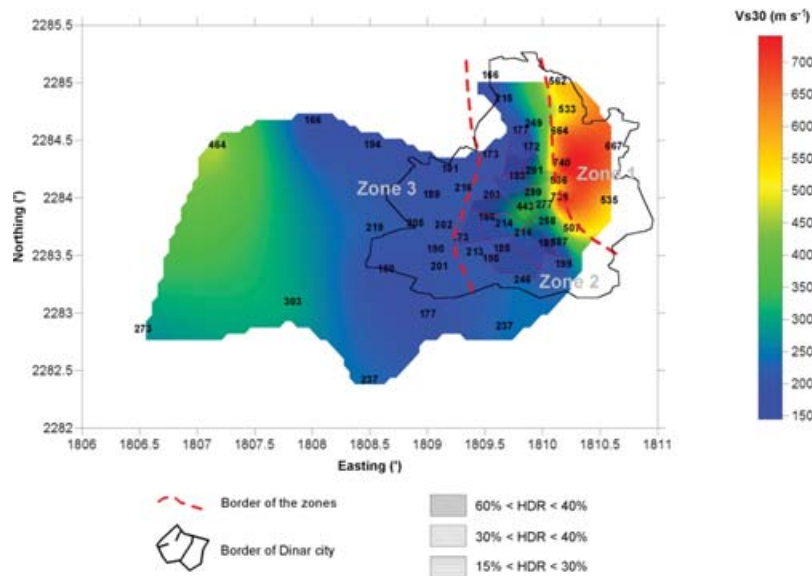
Figure 15. Correlations between the damage distribution of the Dinar earthquake of 1995 October 1 and the distribution of $V_S{}^{30}$ values. The high levels of damage ratios (HDR) are subdivided in levels of damaged area bordered by the red dotted lines.

this zone correspond to better soil types of the UBC and EC8 standards.

8 COMPARISON OF DAMAGE AND $V_S{}^{30}$ DISTRIBUTION

'The proof of the pudding' for the $V_s{}^{30}$ mapping is the comparison of damage and velocity distribution data. The usefulness of soil categories based on shear wave velocities can be illustrated by similarities in damage and velocity distribution patterns. However, several other effects (the quality of buildings, etc.) should also be taken into consideration.

For this comparison previous studies related to the Dinar earthquake and the damage distributions (Bakir *et al.* 2002; Ansal *et al.* 2001; Sucuoğlu *et al.* 2003; Durukal *et al.* 1998), were used. In general, Zone 1 has light or no damage (hill zone—with high $V_S{}^{30}$ velocity values), Zone 2 has the highest damage ratio in the region (alluvial flat basin and transition zone—with low velocity values from the left part of the flat basin to higher $V_S{}^{30}$ velocity values in the transition zone). Finally, in Zone 3 (the western part of Dinar) the level of damage is between the other ones (alluvial flat basin—with low $V_S{}^{30}$ velocity values).

Changes in the $V_S{}^{30}$ velocity values are scattered in the whole flat basin and also in the transition zone, represented by the velocity distribution. For detailed examination a simplified heavy damage distribution map was created from the detailed damage statistics of Durukal *et al.* (1998). This detailed distribution map related only to Zone 2 (Fig. 15). The $V_S{}^{30}$ velocity values and damage index can also be seen in the derived map. High levels of damage ratios (HDR) are subdivided into three main percentage ranges, 15–30, 30–40 and 40–60. Maximum damage ratios concentrate on the centre of the city in the flat alluvial basin and on some fractions towards the transition zone and near the hill zone, forming Zone 2. Generally, the effects of worse geotechnical site conditions on the damage distribution can easily be seen at first glance for the whole region corresponding to the low shear wave velocity distribution. However, the degree of damage ratio is high in some parts of the narrow zone near to the hills and is characterized

by rapid changes in velocity distributions despite the high velocity values.

9 DISCUSSION

Judging from our comparisons, almost the whole flat basin can be characterized by low $V_S{}^{30}$ values. Despite similar soil conditions, the western part of Dinar suffered less damage than the eastern part. Rapid velocity changes, particularly from the transition zone to the hill zone (from Zone 2 to Zone 1), are observed.

It is also clear that the buildings in the western part of Dinar (Zone 3) are quite different from those of the eastern part of the region (Zone 2) in both the number of storeys—which are mostly 1–3 storeys in Zone 3, 1–6 storeys in Zone 2—and the number of buildings (Sucuoğlu *et al.* 2003; Bakir *et al.* 2002). However, the problem related to the damage distribution contrasts in Zone 2 still exists. This situation shows that geotechnical site conditions are not the only reasons of damage distribution but other effects should also be taken into account.

Proceeding eastwards, the basin rapidly gets shallower, starting with the 150 m depth contour in the west in the calculated sediment thickness map derived from the Vs velocity values of this study (Kanlı *et al.* 2004). This situation is known as basin edge structure and Bakir *et al.* (2002) computed the acceleration response spectra taking into account a flat basin without an edge and a basin with an edge and found a significant difference between the two models. The latter yields larger acceleration amplitudes and indicates that the basin edge played an important role in the damage distribution. In addition to this, the shape of the Dinar basin played a key role in the long duration of shaking reported by Kayabalı (1997).

The possible reasons for the damage distribution in the city of Dinar were investigated as follows:

(1) Local soil properties.
(2) Type of buildings.
(3) Resonance frequency.
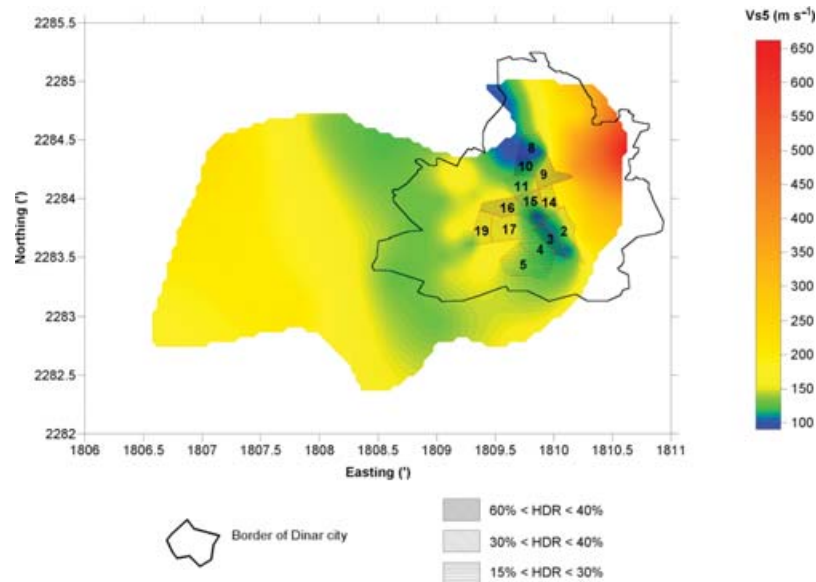(4) Geological inhomogeneities.

Figure 16. Correlations between the damage distribution of the Dinar earthquake of 1995 October 1 and the distribution of V_S^5 values.

(1) *Local soil properties*. This term means the geotechnical parameters of the location. The effects of the geotechnical conditions became very visible in the Dinar region. V_S^{30} is a standard soil classification tool (as in the UBC and EC8 standards). Thus, the V_S^{30} and the damage distribution maps are compared. The damage distribution has been studied in great detail by several authors, who inferred different reasons for it. In general, there is a close correlation between the V_S^{30} and the damage distribution. But the damage distributions at nearby zones that have nearly the same velocities cannot be explained by V_S^{30} or any of the local geotechnical parameters.

(2) *The type of buildings*. The depth of their basements, the quality of the building materials and the structure were not investigated directly. Although both Zone 2 and Zone 3 have low velocity distributions, the damage ratios are quite different. This situation can be explained by the differences of the types of buildings between Zone 2 and Zone 3, but there are also great damage ratio contrasts between the subdivisions of Zone 2. The average velocity distribution of the top 5 m soil (i.e. the effective thickness near to the basements of buildings) was also investigated (Fig. 16), and in some cases a clear correlation can be found between high level of damage and low velocity. However, there are some other subdivisions with no correlation.

(3) *Resonance frequency*. Generally, the damage to the buildings is most severe if the modal frequency of the strata approaches the natural frequency of the building. In Dinar and the surroundings, there were mostly 1–6 storey buildings. Their natural frequencies are in the 1.6–10 Hz range. Microtremor measurements conducted in the region simultaneously with the MASW experiment show that there is no distinct resonance frequency problem in the basin and hill zones. However, the natural frequencies in the transition zone that are between 1.0–5.0 Hz are closer or equal to the natural periods of the buildings, which were mostly between 2–5 storeys (Kanlı *et al.* 2004).

(4) *Geological inhomogeneities*. Geological inhomogeneities mean fast changes in the seismic velocity (geological structure) vertically, horizontally, or both. One plausible explanation for the failure of a satisfactory relationship between Vs and the damage distribution could be the rapid 3-D variation of the Vs velocities. Also, the pattern of damage distribution suggests such a possibility. Our detailed study about the velocity distribution of the Dinar region shows that there is a rapid 3-D variation of the Vs velocities. Between the hill zone and the transition zone, there is a high lateral Vs velocity contrast that may also be one of the underlying causes of damage. An example for a vertical velocity contrast is Profile 14 with a basement close to the surface where heavy damage occurred.

10 CONCLUSIONS

Soil classification results show that most parts of the Dinar region, located in the alluvial basin and exposed to high levels of damage during the earthquake, have low shear wave velocity distribution. That region falls into the S_D category according to the UBC and the C category according to the EC8 standards. Small parts of the region, located on the hill zone and the transition zone, have better soil conditions corresponding to S_C (UBC) and B (EC8) categories and also have higher velocity values than the flat alluvial basin. The worst soil conditions, corresponding to the S_E (UBC) and D (EC8) categories, are also scattered. After conducting a detailed study in the Dinar Region, it is observed that the poor soil condition effects are clear on the damage distribution. In addition, the damage distribution can not be completely predicted by using only the V_S^{30} values, especially in the areas where shear wave velocity values are comparatively high. Detailed soil condition maps based on the shear wave velocity distributions (V_S^{30}) being within the UBC and EC8 standards and the other geotechnical parameters are very important for not only the settlement of the urban areas but also for the site selection and the site safety evaluation studies. These parameters are especially important in the places with high seismic risks such as Turkey.

In other locations, similar to the Dinar region, which have rapid velocity changes in all dimensions, similar tectonic structure and topography, other effects such as the influence of the surroundings and the geometry of the bedrock should be taken into consideration as components of earthquake hazard assessment.

REFERENCES

Aki, K. & Richards, P.G., 1980. *Quantitative Seismology.* W. H. Freeman & Co., San Francisco.

Al-Hunaidi O., 1998. Evolution based genetic algorithm for the analysis of non-destructive surface wave test on pavements, *NDT&F,* **31,** 273–280.

Ansal, A.M., Iyisan, R. & Güllü, H., 2001. Mictrotremor Measurements for the Microzonation of Dinar, *Pure appl. Geophys.,* **158,** 2525–2543.

Bakır, B.S., Özkan, M.Y. & Cılız, S., 2002. Effect of basin edge on the distribution of damage in 1995 Dinar, Turkey Earthquake, *Soil Dyn. Earth. Eng.,* **22,** 335–345.

Barka, A.A., 1992. The North Anatolian fault zone, *Ann. Tectonicae Spec. Issue, Suppl.* **VI,** 164–195.

Ben-Menahem, A. & Singh, S.J., 1981. *Seismic waves and sources.* Springer-Verlag, New York.

Çatal, H.H., 1997. A report on Dinar earthquake of 1 October 1995, and response spectra, *Engineering Structures,* **19,** 594–602.

Clayton, C.R.I., 1995. *The standard penetration test (SPT): methods and use*, CIRIA, London.

Demirtaş, R. *et al.*, 1995. *Preliminary Report on the Dinar Earthquake of October 1, 1995, General Directorate of Disaster Affairs of Turkey*, Earthquake Research Department, Turkey, p. 24.

Dobry, R. *et al.*, 2000. New site coefficients and site classification system used in recent building seismic code provisions, *Earthquake Spectra,* **16,** 41–67.

Dorman, J. & Ewing, M., 1962. Numerical inversion of seismic surface wave dispersion data and crust-mantle structure in the New York-Pennsylvania area, *J. geophys. Res.,* **67,** 5227–5241.

Durukal, E. *et al.*, 1998. Analysis of the strong motion data of the 1995 Dinar, Turkey earthquake, *Soil Dyn. Earthq. Eng.,* **17,** 557–578.

Eyidogan, H. & Barka, A., 1996. The 1 October 1995 Dinar Earthquake, SW Turkey, *Terra Nova* **8,** 479–485.

Forbriger, T., 2003a. Inversion of shallow-seismic wavefields. Part I: Wavefield transformation, *Geophys. J. Int.,* **153,** 719–734.

Forbriger, T., 2003b. Inversion of shallow-seismic wavefields. Part II: Inferring subsurface properties from wavefield transforms, *Geophys. J. Int.,* **153,** 735–752.

Foti, S., Sambuelli, L., Socco, V.L. & Strobbia, C., 2003. Experiments of joint acquisition of seismic refraction and surface wave data, *Near Surface Geophysics,* **1,** 119–129.

Haskell, N.A., 1953. The dispersion of surface waves on multilayered media, *Bull. seism. Soc. Am.,* **43,** 17–34.

Kanlı, A.I., Tildy, P., Prónay, Z. & Pınar, A., 2004. *Quantitative Evaluation of Seismic Site Effects, Final Report (unpublished), Nato Science Programme*, Cooperative Science and Technology Sub-Programme, Collaborative Linkage Grant, Grant Number: EST.CLG.979847.

Kausel, E. & Roesset, J.M., 1981. Stiffness matrices for layered soils, *Bull. seism. Soc. Am.,* **71,** 1743–1761.

Kayabalı, K., 1997. The role of soil behavior on damage caused by the Dinar Earthquake (Southwestern Turkey) of October 1, 1995, *Environ. Eng. Geosci.* **III,** 111–121.

Matthews, M., Hope, V. & Clayton, C., 1996. The use of surface waves in the determination of ground stiffness profiles, In: *Proceedings of the Institution of Civil Engineers, Geotechnical Engineering,* **119,** 84–95.

McMechan, G.A. & Yedlin, M.J., 1981. Analysis of dispersive waves by wave field transformation, *Geophysics,* **46,** 869–874.

Nazarian, S. & Stokoe, K.H. II, 1984. In situ shear wave velocities from spectral analysis of surface waves: In: *Proceedings of the 8th Conference on Earthquake Engineering*, San Francisco, **3,** 31–38.

Nazarian, S., Stokoe, K.H. II, & Hudson, W.R., 1983. Use of spectral analysis of surface waves method for determination of moduli and thicknesses of pavement systems, *Transport. Res. Record,* **930** 38–45.

Öncel, A.O., Koral, H. & Alptekin, Ö., 1998. The Dinar Earthquake ($M_W = 6.2$; October 1, 1995; Afyon-Turkey) and earthquake hazard of the Dinar-Civril Fault, *Pure appl. Geophys.,* **152,** 91–105.

Özpınar, B., 1978. Geophysical Resistivity Investigation Report on the Afyon-Dinar Plain, *18th District of the State Hydraulic Works*, Isparta, Turkey, p. 8.

Park, C.B., Xia, J. & Miller, R.D., 1998. Ground roll as a tool to image near-surface anomaly, *68th Ann. Internat. Mtg., Soc. Expl. Geophys.*, Expanded Abstracts, 874–877.

Park, C.H., Miller, R.D. & Xia, J., 1999. Multichannel analysis of surface waves, *Geophysics,* **64,** 800–808.

Park, C.B., Miller, R.D. & Miura, H., 2002. Optimum field parameters of an MASW survey, *SEG-J*, Tokyo, May 22–23, 2002. Extended Abstracts.

Pınar, A., 1998. Source inversion of the October 1, 1995, Dinar earthquake ($M_S = 6.1$): a rupture model with implications for seismotectonics in SW Turkey, *Tectonophysics,* **292,** 255–266.

Sabetta, F. & Bommer, J., 2002. Modification of the spectral shapes and subsoil conditions in Eurocode 8, *12th European Conference on Earthquake Engineering*, paper ref. 518.

Sêco e Pinto, P.S., 2002. Eurocode 8-Design Provisions for Geotechnical Structures. Special Lecture, *3rd Croatian Soil Mechanics and Geotechnical Engineering Conference*, 2002 Hvar, CD-ROM.

Sen, M.K. & Stoffa, P.L., 1995. *Global Optimization Methods in Geophysical Inversion*, Elsevier, Amsterdam.

Stokoe, K.H. II, Wright, G.W., James, A.B. & Jose, M.R., 1994. *Characterization of geotechnical sites by SASW method, in Geophysical characterization of sites.* ISSMGE Technical Committee #10, ed. Woods, R.D., Oxford Publishers, New Delhi.

Sucuoğlu, H., Anderson, J.G. & Zeng, Y., 2003. Predicting intensity and damage distribution during the 1995 Dinar, Turkey, Earthquake with generated strong motion accelerograms, *Bull. seism. Soc. Am.,* **93,** 1267–1279.

Taymaz, T., Jackson, J. & McKenzie, D., 1991. Active tectonics of the north and central Aegean Sea, *Geophys. J. Int.,* **106,** 433–490.

Tezcan, S. & Ipek, M., 1996. A reconnaissance report: 1995 Dinar, Turkey, *Earthquake. Engineering Structures,* **18,** 906–916.

Thomson, W.T., 1950. Transmission of elastic waves through a stratified solid medium, *J. Appl. Phy.* **21,** 89–93.

Tildy, P., Hermann, L., Neducza, B. & Prónay, Zs., 2003. Seismic Microzoning based on Shear Wave Velocity Measurements. In: *Proceedings of the 9th Meeting of Environmental and Engineering Geophysics*, Prague, P-003.

Wald, L.A. & Mori, J., 2000. Evaluation of Methods for Estimating Linear Site-Response Amplifications in the Los Angeles Region, *Bull. seis. Soc. Am.*, **90**(6B), S32–S42.

Williams, R.A., Stephenson, W.J., Odum, J.K. & Worley, D.M., 1999. S-wave velocities for specific near-surface deposits in Seattle, Washington, *Seis. Res. Lett.* in SSA-99 94th Annual Meeting; Meeting abstracts, **70,** 257.

Wills, J.C., Petersen, M., Bryant, W.A., Reichle, M., Saucedo, G.J., Tan, S., Taylor, G. & Treiman, J., 2000. A Site Condition Map for California Based on Geology and Shear Wave Velocity, *Bull. seism. Soc. Am.,* **90**(6B), 187–208.

Wright, T.J., Parsons, B.E., Jackson, J.A., Haynes, M., Fielding, E.J., England, P.C. & Clarke, P.J., 1999. Source parameter of the 1 October 1995 Dinar (Turkey) earthquake from SAR interferometry and seismic body-wave modelling, *Earth planet. Sci. Lett.,* **172,** 23–37.

Xia, J., Miller, R.D. & Park, C.B., 1999. Estimation of near-surface shear-wave velocity by inversion of Rayleigh wave, *Geophysics,* **64,** 691–700.

Xia, J., Miller, R.D., Park, C.B., Hunter, J.A., Harris, J.B. & Ivanov, J., 2002. Comparing shear-wave velocity profiles inverted from multichannel surface wave with borehole measurements, *Soil Dyn. Earthq. Eng.* **22,** 181–190.